



Article

Myocardial Remodeling in Early Chronic Kidney Disease—Mineral and Bone Disorder Model with Low Bone Turnover

Evdokia Bogdanova ^{1,*} , Airat Sadykov ², Galina Ivanova ³ , Irina Zubina ¹, Olga Beresneva ¹, Olga Galkina ¹, Marina Parastaeva ¹, Vladimir Sharoyko ⁴ and Vladimir Dobronravov ¹

- ¹ Research Institute of Nephrology, Pavlov University, 197022 Saint Petersburg, Russia; zubina@list.ru (I.Z.); beresnevaolga@list.ru (O.B.); ovgalkina@mail.ru (O.G.); orcid0000000275322405@gmail.com (M.P.)
² Raisa Gorbacheva Memorial Research Institute for Pediatric Oncology, Hematology and Transplantation Pavlov University, 197022 Saint Petersburg, Russia; bmt-director@1spbmu.ru
³ Laboratory of Cardiovascular and Lymphatic Systems, Physiology Pavlov Institute of Physiology, 199034 Saint Petersburg, Russia; tazhim@list.ru
⁴ Department of General and Bioorganic Chemistry, Pavlov University, 197022 Saint Petersburg, Russia; kafedrachemistry@yandex.ru
* Correspondence: evdokia.bogdanova@gmail.com

Abstract: Chronic kidney disease—mineral and bone disorder (CKD-MBD) plays a significant role in causing cardiovascular morbidity and mortality related to CKD. CKD-MBD has been studied during advanced stages when changes in inorganic phosphate (Pi) and its hormonal regulation are obvious. The initial phases of myocardial remodeling (MR) in early CKD-MBD remain poorly understood. We induced mild CKD-MBD in spontaneously hypertensive rats using 3/4 nephrectomy. Animals were fed standard chow, containing 0.6% phosphate. In each animal, we analyzed indices of chronic kidney injury, bone turnover and Pi exchange, and assessed the myocardial histology and gene expression profile. Applied CKD-MBD models corresponded to human CKD S1-2 with low bone turnover and without an increase in systemic Pi-regulating factors (parathyroid hormone and fibroblast growth factor 23). In mild CKD-MBD models, we found MR features characterized by cardiomyocyte hypertrophy, interstitial and perivascular fibrosis, intramyocardial artery media thickening, along with alterations in *Ppp3ca*, *Mapk1*, *Jag1*, *Hes1*, *Ptch1*, *Numb*, *Lgr4* and *Bmp4* genes. Among other genes, the down-regulation of *Jag1* was most tightly associated with either myocardial hypertrophy or fibrosis. Myocardial alterations concurrently occurred with mild CKD-MBD and comprised fibrosis preceding cardiomyocyte hypertrophy. The histological features of MR were associated with myocardial P accumulation in settings of low bone turnover, prior to a response of systemic Pi-regulating factors and with alterations in calcineurin, ERK1/2, Notch, BMP and Hedgehog genes.

Keywords: chronic kidney disease—mineral and bone disorder; myocardial remodeling; phosphate; calcineurin; ERK1/2; PiT-2; Jagged1; Patched 1; *Hes1*; *Lgr4*



Citation: Bogdanova, E.; Sadykov, A.; Ivanova, G.; Zubina, I.; Beresneva, O.; Galkina, O.; Parastaeva, M.; Sharoyko, V.; Dobronravov, V. Myocardial Remodeling in Early Chronic Kidney Disease—Mineral and Bone Disorder Model with Low Bone Turnover. *Kidney Dial.* **2023**, *3*, 322–334. <https://doi.org/10.3390/kidneydial3040028>

Academic Editor: Francesco Locatelli

Received: 1 August 2023

Revised: 26 September 2023

Accepted: 28 September 2023

Published: 3 October 2023



Copyright: © 2023 by the authors. Licensee MDPI, Basel, Switzerland. This article is an open access article distributed under the terms and conditions of the Creative Commons Attribution (CC BY) license (<https://creativecommons.org/licenses/by/4.0/>).

1. Introduction

Patients with chronic kidney disease (CKD) exhibit significantly increased cardiovascular risks [1–3], and heart failure is a leading cause of morbidity and mortality among them [4–6]. Mineral and bone disorder in CKD (CKD-MBD) is thought to be an important contributor to the progression of cardiomyopathy, in addition to other CKD-related mechanisms [7–10]. Studies of CKD-MBD have mainly focused on later disease stages. Being apparent at these stages, high levels of serum inorganic phosphate (Pi), parathyroid hormone (PTH), fibroblast growth factor 23 (FGF23) and Klotho depression may themselves impact heart remodeling and bone turnover [11–22]. Notably, the extent of kidney

dysfunction and trends in Pi exchange dysregulation may result in different bone phenotypes, either with high or low bone turnover. Among them, a statement with low bone turnover is prevalent (Table S1) [23–25]. As widely accepted, myocardial hypertrophy is a hallmark of cardiac remodeling and dysfunction in CKD [23–25]. Concurrently, interstitial fibrosis and extensive alterations of cardiac microcirculation represent a significant impact on myocardial remodeling (MR) in an overt CKD setting [26–30].

Myocardial hypertrophy in overt CKD is known to be associated with angiotensin II, catecholamines, hyperphosphatemia, hyperparathyroidism, an increase in FGF23 and Klotho decline and is mediated by various signaling pathways, including calcineurin, mitogen-activated protein kinase ERK1/2, calmodulin-dependent protein kinase II, etc. [31–34].

Being less understood, the mechanisms of fibrosis in CKD might be related to hyperphosphatemia and a decrease in renal and systemic Klotho, as well as to locally produced growth factors, cytokines, chemokines, miRNA and bone-derived circulatory factors [29,35–37].

The pathogenesis of early CKD-MBD without hyperphosphatemia, hyperparathyroidism and increased serum FGF23 levels and its cardiovascular consequences remain largely unexplored (Table S1). Understanding the early mechanisms of MR could be of importance in determining molecular targets to prevent irreversible myocardial disease in overt CKD-MBD.

In line with the above, our study aimed to identify whether MR occurs in mild CKD-MBD without an increase in systemic Pi-regulating factors (PTH, FGF23) associated with CKD. Our data confirmed the presence of the histological features of MR—cardiomyocyte hypertrophy, interstitial fibrosis and vascular remodeling, along with alterations in gene expression profiles related to hypertrophy and fibrosis.

2. Materials and Methods

2.1. Animals

The study was conducted according to the Code of practice for the housing and care of animals bred, supplied or used for scientific purposes [38] and approved by the local Ethics Committee of Pavlov University (animal ethics approval code No. 02-2013, 23 April 2018) and adhered to the European Community Council Directive (2010/63EU) [39] and the guidelines of the National Institute of Health (Guide for the Care and Use of Laboratory Animals) [40].

Adult male spontaneously hypertensive rats (SHR) and Wistar Kyoto (WKY) rats (Table S2) were housed using a 12-h/12-h daylight cycle at room temperature (20–22 °C) with ad libitum access to water and standard rat chow containing 0.6% phosphate.

We induced mild CKD in SHR by arterial hypertension (AH) exposure combined with a sham operation (SO) or 3/4 nephrectomy (Nx) (Table 1, Figure S1).

Table 1. Correlation analysis of the association between the histology indexes of myocardial remodeling and the parameters of phosphate balance.

	Cardiomyocyte Diameter, Mcm	Media Thickness, Mcm	Perivascular Fibrosis, Mcm	Myocardial Interstitial Fibrosis, %
Myocardial P, mg/kg	−0.34 <i>p</i> = 0.17	0.52 <i>p</i> = 0.029	−0.41 <i>p</i> = 0.09	0.13 <i>p</i> = 0.60
Serum phosphate, mmol/L	0.58 <i>p</i> = 0.012	0.68 <i>p</i> = 0.002	0.65 <i>p</i> = 0.003	0.50 <i>p</i> = 0.026
Fractional phosphate excretion, %	0.21 <i>p</i> = 0.38	0.14 <i>p</i> = 0.59	0.38 <i>p</i> = 0.041	0.35 <i>p</i> = 0.16
PTH, pg/mL	0.60 <i>p</i> = 0.008	−0.20 <i>p</i> = 0.42	0.27 <i>p</i> = 0.27	0.11 <i>p</i> = 0.65
FGF23, pg/mL	0.21 <i>p</i> = 0.39	−0.37 <i>p</i> = 0.13	−0.05 <i>p</i> = 0.83	−0.18 <i>p</i> = 0.48
Serum Klotho, pg/mL	−0.33 <i>p</i> = 0.12	−0.22 <i>p</i> = 0.37	0.12 <i>p</i> = 0.64	−0.22 <i>p</i> = 0.19

SHR with two-month AH exposure served as controls (SO2). We obtained three groups of experimental mild CKD: (i) AH-induced in sham SHRs with six-month exposure (SO6); (ii) AH and Nx with two-month exposure (Nx2); and (iii) AH and Nx with six-month exposure (Nx6). As hypertension is a kidney injury factor in SHRs, we also used a sham Wistar Kyoto with a 2-month follow-up (WKY2) as a normotensive control. Additional purposes for using the WKY2 group was to confirm that the SO2 group had normal kidney function, heart remodeling and phosphate exchange indexes (compared to normotensive WKY2). Since Wistar Kyoto and SHR are genetically different strains, we did not use the WKY2 group to compare gene expression to SHRs. Between SHR groups, we made the following comparisons: control SO2 vs. all mild CKD groups (SO6, Nx2, Nx6); earlier stages of mild CKD (SO6) vs. Nx2 and Nx6; and Nx2 vs. Nx6.

Systolic blood pressure was measured the day before the euthanasia using the tail-cuff method using an electrometer (ELEMA, Lund, Sweden) and registered at a paper speed of 10 mm/s.

Blood, left-side kidney, left-side tibia and myocardial samples were harvested immediately after sacrifice. The myocardial mass index (MMI) was calculated as a ratio of the myocardium mass (mg) to the mass of the rat (g); 24-h urine samples were collected the day before.

2.2. Laboratory Measurements

The blood and 24-h urine samples were centrifuged at 3000 rpm for 10 min, aliquoted and stored at -80°C with temperature control. The stored samples underwent a single thaw followed by assays. The levels of creatinine (using the enzymatic method) and Pi were measured using reagent kits on SYNCHRON CX DELTA (Beckman Coulter, Brea, CA, USA) following calculations of fractional Pi excretion (FEPi) and absolute urinary Pi excretion (urinary Pi/urinary Cr). We estimated the serum phosphorus (P) content per rat as:

$$P \text{ (mg/rat)} = (s\text{Pi} \cdot \text{Ar(P)} \cdot \text{BV} \cdot \text{m})/1000, \quad (1)$$

where: sPi—concentration of serum inorganic phosphate (mmol/L), Ar(P)—atomic weight of phosphorus (30.97 g/mol), BV—average blood volume per 1 kg for rodents (0.06 L) [41], m—rat body weight (g).

The levels of urinary albumin were measured by immuno-turbidimetry using reagent kits (Vital, Saint Petersburg, Russia) on an CA-90 analyzer (Furuno, Nagasaki, Japan). Albuminuria was calculated as a ratio of the urinary albumin to the urinary creatinine.

The levels of intact PTH and intact FGF23 were measured using a MILLIPLEX MAP «Rat Bone Magnetic Bead Panel 1» (EDM Millipore Corporation, Billerica, MA 01821, USA) on a Bio-Plex 200 Reader (Bio-Rad, Hercules, CA, USA), and a serum α -Klotho—using an ELISA Kit for Rat (Cloud-Clone Corp., Katy, TX, USA) on a Microplate Reader Immunochem 2100 (High Technology, North Attleborough, MA, USA).

2.3. Inductively Coupled Plasma Atomic Emission Spectroscopy

The tibial diaphysis, myocardial wall and kidney cortex were sampled and stored at -80°C with temperature control. An inductively coupled plasma-atomic emission spectrometry method was used for the measurement of phosphorus in the bones and kidneys. The specimens were mineralized using nitric acid (Merck, Darmstadt, Germany) with subsequent microwave decomposition: a temperature-time ramp for 20 min with a final temperature of 210°C , then a 25-min hold time at 1500 W at 210°C . The analysis was performed with an ICPE-9000 (Shimadzu, Kyoto, Japan) with the following parameters: radio frequency power of 1550 W, sample depth of 10 mm, carrier gas at 0.65 L/min, nebulizer pump at 0.10 rps, spray chamber temperature at 13°C (55.4°F) and dilution gas at 0.40 L/min as previously described [42]. The phosphorus content in the kidney and myocardium was calculated considering the kidney or myocardial mass.

2.4. Real-Time Polymerase Chain Reaction

Samples of tibial diaphyses and myocardium were flushed with phosphate-buffered saline, incubated overnight at 4 °C with RNAlater (Evrogen, Moscow, Russia) and stored at −80 °C with temperature control. Total RNA was extracted using the TriZ reagent RNA Kit (Inogene, Saint Petersburg, Russia) following the manufacturer's instructions. The extracted RNA was eluted in RNase-free water. A reverse transcriptase reaction was performed using a RevertAid First Strand cDNA Synthesis Kit (Thermo Scientific, Waltham, MA, USA). For each generated cDNA sample, multiplex qPCR was performed for genes of interest and glyceraldehyde-3-phosphate-dehydrogenase (Table S2). All reactions were adapted from the manufacturer's protocol (Syntol, Moscow, Russia, M-428), containing 2.5 mM of each dNTP, ×10PCR buffer, 5 units of Taq-DNA polymerase, and 2.5 µL of 25 mM MgCl₂, supplemented with 7 pmol of each genespecific primer, 5 pmol of Taqman probes for the genes of interest and glycer-aldehyde-3-phosphate-dehydrogenase. The final reaction volume was 25 µL. Quantitative real-time PCR was performed using a BioRad CFX 96 (BioRad, Hercules, CA, USA). The amplification protocol was 95 °C for 10 min, followed by 45 cycles of heating at 95 °C for 15 s, annealing at 60 °C for 1 min and signal detection. We performed an in silico search for potential molecules involved in myocardial and vascular remodeling using the Search Tool for Recurring Instances of the Neighboring Genes Database to predict interaction networks and the biological processes in which they are were involved "<https://string-db.org/>" (accessed on 15 March 2023)". The relative expression gene of interest level was calculated using the Delta Ct method and expressed as a percent value. All PCR results for one gene in one animal represented mean values of triplicated measurements for each mRNA level. Studied genes, including differentially expressed ones, were further analyzed.

2.5. Histology

Kidney, myocardium and tibial distal metaphysis with diaphysis were fixed in buffered 4% formaldehyde for 24 h, 24 h and 48 h, respectively. Afterward, tibial samples were incubated with 10% EDTA (pH 7.4) for around two months. The EDTA solution was replaced twice a week. Processed tissues were embedded in paraffin and cut into two-micron sections, dewaxed, rehydrated and stained. Staining included standard hematoxylin and eosin, PAS or Masson's staining.

2.6. Quantitative Morphometry

Renal, myocardial and bone histomorphometric parameters were quantitatively calculated with the two examiners blinded to the study groups who examined ten fields of view (400× magnification, 10×/22) for a section or in a whole slide image using the freeware Orbit Image Analysis Version 3.64 and Panoramic Viewer 1.15.4.

The area of renal interstitial fibrosis (Masson's trichrome) was measured at the renal cortex sites without glomeruli in ten random fields of view for one slide per rat and expressed as a percent using Orbit Image Analysis. The mean values for each animal were analyzed afterward.

Bone histomorphometric parameters were measured in compliance with «Bone research protocols, Methods in molecular biology (Histomorphometry in Rodents)» [43] and the recommendations of the nomenclature committee of the American Society for Bone and Mineral Research [44].

To quantify the bone area in the metaphyseal region, the trabecular bone area and bone tissue area were measured in three whole slide images for sections spaced at least 100 µm from each other for one animal. The trabecular bone area was standardized to a bone tissue area (B.Ar%T.Ar), and the mean values of the three measurements for each animal were analyzed (N = 96 [32 animals × 3 whole slide images], n = 8 for each group). For the areas of bone marrow cells, adipose cells were included in three whole slide images for sections spaced at least 100 µm from each other for one animal. The ratio of bone marrow cells to adipose for each animal was used for further statistical tests.

The number of active osteoblasts (N.Ob) and osteoclasts (N.Oc), the eroded perimeter (E.Pm) and bone perimeter (B.Pm) in the metaphyseal region and the number of osteocytes (N.Ot) in the diaphyseal region were calculated in 8–10 fields of view for each animal. N.Ot were standardized to the bone tissue area. N.Ob, N.Oc and E.Pm were standardized to B.Pm. The mean values for each animal were analyzed afterward.

The left ventricular wall thickness, cardiomyocyte diameter (H&E) and myocardial interstitial fibrosis were measured on the areas without intramyocardial arteries and veins (Masson's staining); intramyocardial artery media and perivascular fibrosis were quantitatively scored in 10 fields of view (200× magnification) in one section for each animal using Panoramic Viewer 1.15.4.

2.7. Statistical Analyses

Analyses were performed using SAS version 9.4 (SAS Institute Inc., Cary, NC, USA). Values are expressed as medians [interquartile range (IQR)]. Groups were compared using the two-tailed Mann-Whitney U test or the Kruskal Wallis test. The association between variables was evaluated in the SHR group using Spearman's coefficient. Statistical significance was defined at p -values < 0.05.

3. Results

3.1. Animal Models of Chronic Kidney Disease—Mineral and Bone Disorder with Low Bone Turnover

All experimental groups (SO6, Nx2, Nx6) demonstrated an increase in serum creatinine (Cr), albuminuria the area of renal interstitial fibrosis (IF), and a decline in the serum Klotho level (Figure S1, Table S3). In SO2 controls, all these renal indices were the same as in the normotensive control (WKY2), indicating intact kidney function in SO2 rats (Figure S1, Table S3). In experimental groups (SO6, Nx2, Nx6), albuminuria increased by 6–12-fold, while values of serum Cr and renal IF were <30% compared to the controls, suggesting similarity of the applied experimental models to human CKD S1-2. SO6 was further sub-classified as having the earliest chronic kidney injury (Figure S1). Compared to SO6, Nx2 and Nx6 corresponded to intermediate and more pronounced chronic kidney injury, respectively (Figure S1).

Regarding the bone, a significant decrease in the trabecular bone area and osteocyte number (SO6, Nx2, Nx6), osteoblast number (Nx2, Nx6) and eroded perimeter (Nx6) showed in the CKD-MBD models (Figure S2). There were no differences in osteoclast number and the ratio of bone marrow cells to adipose tissue between groups (Figure S2). Notably, a bone histology alteration was associated with the significant down-regulation in genes related to osteogenesis (*Sp7*, *Ctnnb1*, *Bmp4*, *Vdr*) (Figure S3). Collectively, bone histomorphometric studies and gene expression profiles were suggestive of low bone formation in the applied CKD-MBD models.

The serum Pi and total serum phosphorus (P) content per rat were higher in Nx6 compared to the control (SO2) and experimental groups (SO6, Nx2; Table S2). Kidney and bone tissue P concentration remained unchanged, while myocardial P was higher in nephrectomized animals (Table S2). The fractional excretion of Pi (FEPi) increased in Nx groups (Nx2, Nx6) (Table S2). There were no changes in absolute urinary Pi excretion, as well as in levels of serum PTH and FGF23 (Table S2).

3.2. Myocardial Remodeling in Applied CKD-MBD Models

The myocardial mass index (MMI) and histological parameters of heart remodeling—left ventricular wall thickness (LVWT), cardiomyocyte diameter (CMD), interstitial (MF) and perivascular fibrosis and thickness of intramyocardial artery (IA) media—in the hypertensive controls (SO2) were similar to normotensive rats (WKY2), suggesting normal myocardial morphology in SO2 (Table S2, Figure 1).

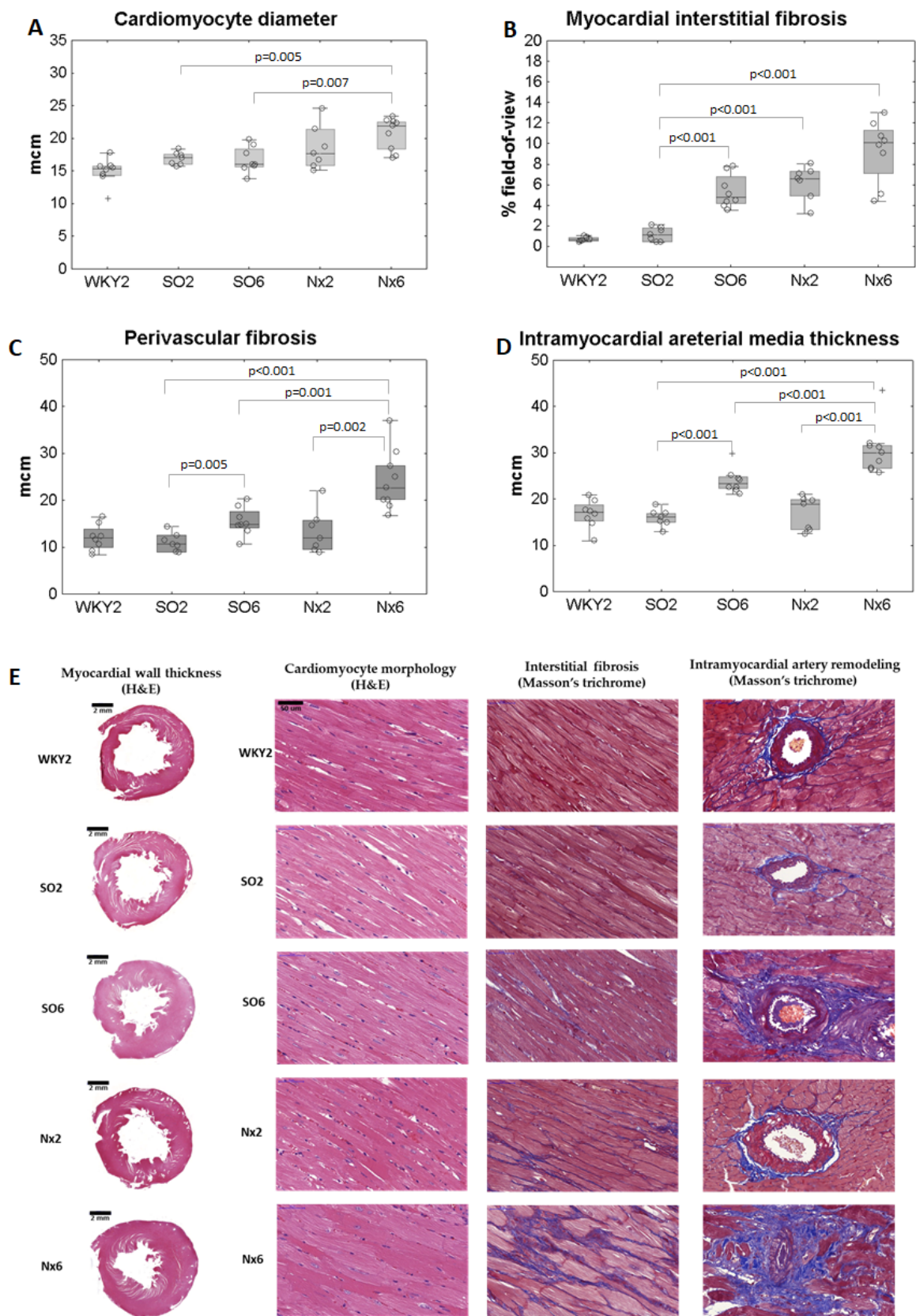


Figure 1. Parameters of myocardial histology: the quantitative morphometry for (A)—cardiomyocyte diameter; (B)—myocardial interstitial fibrosis; (C)—intramyocardial artery perivascular fibrosis; (D)—intramyocardial artery media thickness; (E)—representative microphotographs for morphometry parameters of myocardium; raw data shown as “circles”, outliers shown as “+”.

MMI, LVWT and CMD were higher in Nx6 (Table S2, Figure 1A,E). An increase in the area of MF was obvious in Nx6 with more pronounced CKD-MBD, and even in SO6, Nx2 models with a lesser extent of the disease (Figure 1B). The perivascular fibrosis and thickness of IA media increased in both SO6 and Nx6 groups, being most prominent in the latter (Figure 1C,D). Media remodeling exhibited smooth muscle cell hypertrophy and collagen deposition without features of its calcification (Figure S4).

3.3. Myocardial Histology and Phosphate Indexes

In pooled analyses of the SHRs group, all histological indices of myocardial and vascular remodeling positively correlated with the serum Pi level (Table 1). In addition, we found correlations between the thickness of IA media and myocardial P content; IA perivascular fibrosis and fractional phosphate excretion; cardiomyocyte diameter and serum PTH level (Table 1).

3.4. Gene Expression Profile Related to Myocardial Hypertrophy and Fibrosis in Mild CKD-MBD

Among the genes studied (Figure 2A), we found significant alterations in the expression of calcineurin catalytic subunit A (*Ppp3ca*), mitogen-activated protein kinase ERK1/2 (*Mapk3*, *Mapk1*), solute carrier family 20 member 1 (PiT-1, *Slc20a1*), Notch pathway components (*Jag1*, *Hes1*, *Numb*), Hedgehog negative regulator Patched 1 (*Ptch1*), leucine-rich repeat-containing G-protein-coupled receptor 4 (*Lgr4*) and bone morphogenetic protein 4 (*Bmp4*) (Figure 2B).

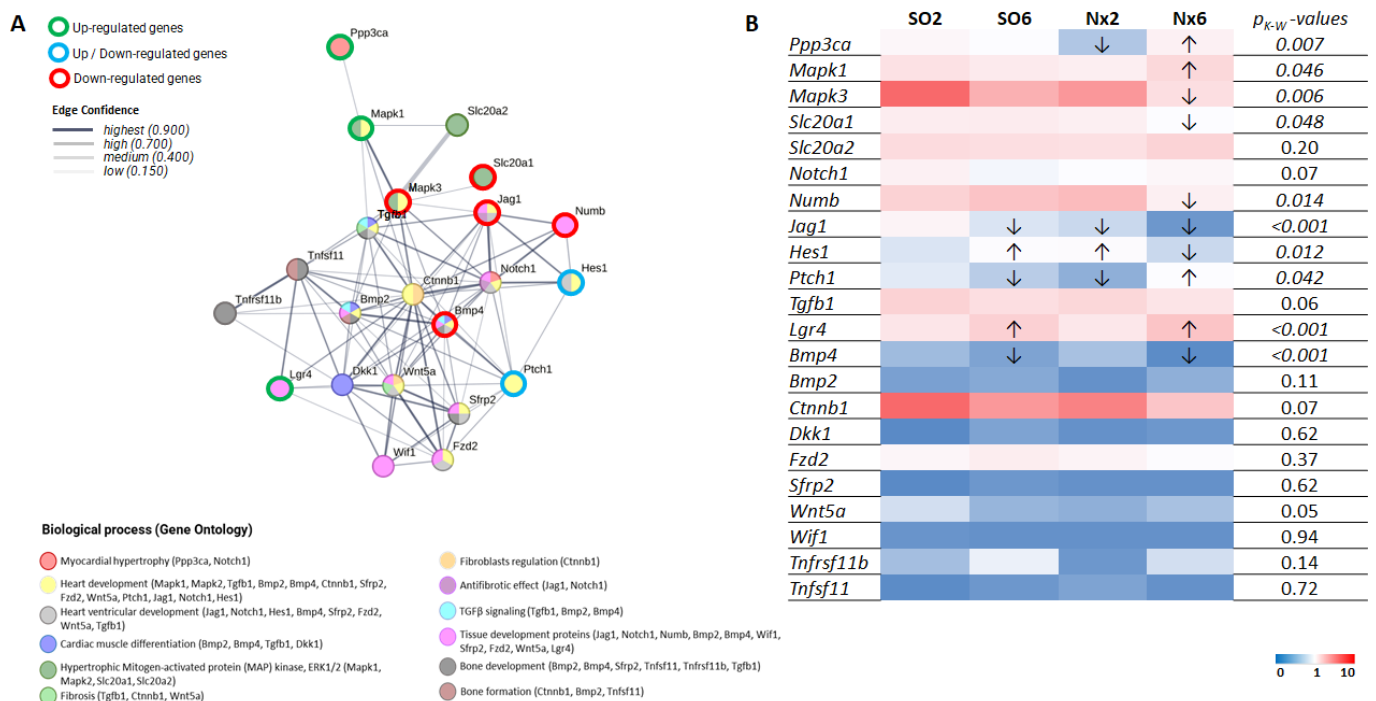


Figure 2. Myocardial gene expression profile in mild CKD-MBD: (A)—Predicted interactions between studied gene products (STRING Database: <https://string-db.org/> (accessed on 15 March 2023)); a network for studied gene profile involved in major biological processes of cardiac regulation, heart hypertrophy, fibrosis; (B)—mRNA relative expression in the myocardium of the control (SO2) and mild CKD (SO6, Nx2, Nx6) groups; *p_{K-W}*—*p*-value for Kruskal Wallis test.

Ppp3ca, calcineurin A; *Mapk1*, mitogen-activated protein kinase 1 (Erk2); *Mapk3*, mitogen-activated protein kinase 3 (Erk1); *Slc20a1*, solute carrier family 20 member 1 (PiT-1); *Slc20a2*, solute carrier family 20 member 1 (PiT-2); *Notch1*, notch receptor 1; *Numb*, NUMB endocytic adaptor protein; *Jag1*, jagged canonical Notch ligand 1; *Hes1*, hes family bHLH transcription factor 1; *Ptch1*, patched 1; *Tgfb1*, transforming growth factor beta 1;

Lgr4, leucine-rich repeat-containing G protein-coupled receptor 4; *Bmp4*, bone morphogenetic protein 4; *Bmp2*, bone morphogenetic protein 2; *Ctnnb1*—catenin beta 1; *Dkk1*, dickkopf 1; *Fzd2*, frizzled class receptor 2; *Sfrp2*, secreted frizzled-related protein 2; *Wnt5a*, Wnt family member 5A; *Wif1*, Wnt inhibitory factor 1; *Tnfrsf11B*, TNF receptor superfamily member 11 B (OPG); *Tnfsf11*, TNF superfamily member 11 (RANKL); arrows show direction of statistically significant differences in gene expression compared to the control or other CKD-MBD groups with lower injury.

In Nx6, *Ppp3ca* and *Mapk1* expression were up-regulated, while *Numb*, *Mapk3* and *Slc20a1* were down-regulated vs. the SO6 and Nx2 subgroups and the control (Figure 2B). LVWT positively correlated with *Ppp3ca* and *Mapk1*, and negatively with Notch genes (*Notch1*, *Jag1*, *Hes1*, *Numb*) and *Bmp4* (Table 2). *Mapk1* expression correlated with *Slc20a2* ($r = 0.60$, $p = 0.015$); *Numb* was directly associated with *Ctnnb1* ($r = 0.63$, $p = 0.019$).

Table 2. Correlation analysis of gene profile and myocardial histology in pooled SHR group.

	Left Ventricular Wall Thickness	Myocardial Interstitial Fibrosis	Vascular Media Thickness	Perivascular Fibrosis
<i>Mapk1</i>	0.43 *	0.33	0.39 *	0.33
<i>Mapk3</i>	−0.27	−0.23	−0.33	−0.32
<i>Notch1</i>	−0.35 *	0.24	−0.34	−0.33
<i>Numb</i>	−0.45 *	−0.49 *	−0.51 *	−0.54 *
<i>Ppp3ca</i>	0.44 *	0.02	0.14	0.05
<i>Slc20a1</i>	−0.32	−0.34	−0.34	−0.34
<i>Slc20a2</i>	−0.05	−0.07	0.14	0.01
<i>Ctnnb1</i>	−0.22	0.26	−0.32	−0.23
<i>Jag1</i>	−0.46 *	−0.71 *	−0.70 *	−0.72 *
<i>Hes1</i>	−0.43 *	−0.34	−0.45 *	−0.42 *
<i>Ptch1</i>	0.20	−0.41	0.14	−0.04
<i>Tgfb1</i>	−0.12	−0.22	−0.34	−0.19
<i>Lgr4</i>	−0.12	0.18	0.71 *	0.52 *
<i>Bmp4</i>	−0.36 *	−0.34	−0.69 *	−0.57 *

Mapk1, mitogen-activated protein kinase 1 (Erk2); *Mapk3*, mitogen-activated protein kinase 3 (Erk1); *Notch1*, notch receptor 1; *Numb*, NUMB endocytic adaptor protein; *Ppp3ca*, calcineurin A; *Slc20a1*, solute carrier family 20 member 1 (PiT-1); *Slc20a2*, solute carrier family 20 member 1 (PiT-2); *Ctnnb1*—catenin beta 1; *Jag1*, jagged canonical Notch ligand 1; *Hes1*, hes family bHLH transcription factor 1; *Ptch1*, patched 1; *Tgfb1*, transforming growth factor beta 1; *Bmp4*, bone morphogenetic protein 4; *— $p < 0.05$.

Jag1 was down-regulated in all CKD-MBD models (Figure 2B). Its mRNA level was inversely associated with interstitial and perivascular fibrosis and media hypertrophy (Table 2).

Hes1 was up-regulated in SO6 and Nx2 and down-regulated in a more pronounced CKD-MBD group, Nx6 (Figure 2B). *Hes1* correlated with *Ptch1* ($r = -0.52$, $p = 0.035$) and *Bmp4* expression ($r = 0.66$, $p = 0.005$).

Bmp4 was down-regulated and *Lgr4* was up-regulated in SO6 and Nx6 (Figure 2B) both correlated with IA remodeling (Table 2) and serum Pi level (*Lgr4*: $r = 0.48$, $p = 0.040$; *Bmp4*: $r = -0.52$, $p = 0.037$).

4. Discussion

In this exploratory study, we focused on histological and molecular alterations of the myocardium in experimental CKD-MBD. Notably, we applied CKD-MBD models with the earliest possible stages of the disease. Corresponding to S1-2 stages of human CKD, experimental animals already had features of Pi imbalance and bone turnover lowering, however, without a significant increase in serum PTH and FGF23 levels.

First, we definitively confirmed the occurrence of MR concurrently with bone and kidney dysfunction. The former was characterized by left ventricular hypertrophy and diffuse interstitial myocardial fibrosis, in line with the findings of other studies, mostly performed in advanced CKD [2,4–10,45–47].

Here, we showed that fibrosis is an early event in CKD-MBD-related cardiomyopathy, preceding hypertrophy. Interstitial and perivascular fibrosis were already obvious in models with less prominent renal and bone lesions (SO6, Nx2). Conversely, myocardial hypertrophy was only detected in Nx6, which was more pronounced amongst the CKD-MBD models applied. In addition to fibrosis, an early event of CKD-MBD was IA media thickening due to smooth muscle cell hypertrophy and collagen deposition without vascular calcification.

Then, we found that MR might arise in the settings of renal-induced early Pi imbalance. In addition to lowering sKlotho, the latter was characterized by an increase in FEPi, but without alterations in absolute urinary Pi excretion, serum Pi (at least in SO6 and Nx2 models), PTH and FGF23.

One should take into consideration features of lower bone turnover in all of the applied CKD-MBD models. As the hydroxyapatite of the long bones serves as a huge natural reservoir for Pi [48], low bone turnover may predispose the redistribution of Pi to non-skeletal tissues. Myocardium could be prone to Pi accumulation because of the ability of myocytes to accumulate high amounts of this anion, which is necessary to maintain their high-energy metabolism [49]. The findings of a recent study on human CKD suggested that muscle tissues can serve as a phosphorus reservoir, alongside bones [50].

In line with this concept, we found particularly high myocardium P content in nephrectomized animals. It seems to be interesting that an increase in P occurred either with (in Nx6) or without (Nx2) hyperphosphatemia, a hallmark of significant Pi retention. That myocardial phosphorus content was correlated with the media thickness of intramyocardial arteries might suggest this myocardial compartment is more vulnerable to Pi retention in mild CKD-MBD. The intriguing results of our study suggested myocardial phosphorus shifting in the settings of insidious renal Pi retention as one of the potential triggers of MR, including the vascular compartment. The molecular mechanisms of MR associated with myocardial Pi retention in CKD-MBD require further studies.

Our study shed some light on the likely molecular basis of early-stage CKD-MBD-induced MR. Up-regulation in genes related to pro-hypertrophic pathways *Ppp3ca* (calcineurin catalytic subunit A) [30] and *Mapk1* (ERK2) [32] accompanied myocardial hypertrophy in CKD-MBD (Nx6). In the earlier Nx2 model, characterized by MF without obvious myocardial hypertrophy, the expression of *Ppp3ca* was down-regulated. This finding is relevant to the other data shown in the calcineurin suppression in MR, not manifested by hypertrophy [51,52]. The correlation of serum Pi with *Mapk1* (ERK2) and *Slc20a2* (PiT-2) was in line with prior data on the Pi/PiT-1/2-dependent activation of the ERK1/2 pathway [53–55] involved in myocardial hypertrophy followed by Pi retention [32]. Levels of *Slc20a1* (PiT-1), the main Pi transporter, had no correlation with serum Pi, PTH, FGF23 or myocardial histological lesions and gene expression. These findings might be related to a different role of PiT-2 and PiT-1 in the pathogenesis of MR in a state of Pi retention.

All CKD-MBD models were characterized by a decrease in myocardial *Jag1* expression. *Jag1* encoding Notch ligand *Jagged1*, which is crucial for CKD-independent MR [51,53–55]. Notch depression may also contribute to the maladaptive cardiac response in early CKD-MBD, as the down-regulation in Notch genes was associated with hypertrophy, fibrosis and a thickening of the IA media (see Table 2).

In mild CKD-MBD models (SO6, Nx6), we found vascular remodeling to be likely associated with *Lgr4* expression. LGR4 is a receptor for R-spondins, which potentiates the canonical Wnt pathway and is involved in the regulation of adult stem cell homeostasis. *Lgr4* increases in hypertrophic hearts and may drive a pro-inflammatory program of macrophages during post-infarction heart repair [56]. In a single study of non-CKD-dependent cardiovascular disease, *Lgr4* expression was also associated with β -catenin

signals promoting vascular fibrosis in a single study of non-CKD-dependent cardiovascular disease [57].

Another finding of the study was that the myocardial phenotype, including non-calcified IA remodeling in CKD-MBD, is associated with a decrease in *Bmp4* expression. In contrast, other studies have suggested up-regulated bone morphogenetic proteins, *BMP2* and *BMP4*, to be involved in cardiac hypertrophy and vascular calcification states in ischemia, overload and metabolic and genetic models [58–60].

Cross-talks between various pathways might have an impact on the progression of MR in CKD-MBD. The expression of *Hes1*, the coding HES1 transcription factor (the effector of the Notch pathway), negatively correlated with *Ptch1* and positively with *Bmp4*, assuming the non-canonical *Hes1* activation by the BMP and/or Hedgehog pathways in early MR induced by CKD-MBD [61–64]. Although *Ctnnb1* expression did not differ in CKD-MBD, we found its direct association with *Numb*. TCF/LEF-binding sites were identified within the NUMB promoter based on bioinformatics, which predisposed regulation by canonical Wnt signaling [65]. NUMB acts as a Notch antagonist by controlling the intracellular destination and stability of the ligand Delta-like 4 and interactions with the Notch intracellular domain (NICD) [66]. These data might suggest the role of WNT and Notch in the pathogenesis of MR in CKD-MBD. However, further studies are needed to confirm these assumptions.

To the best of our knowledge, the present study is the first aiming to evaluate how mild CKD-MBD may contribute to early cardiac remodeling. This knowledge may be useful for further experimental modeling or translation in clinical research to determine new early molecular targets and develop therapeutic strategies preventing CKD-MBD-induced cardiomyopathy.

5. Conclusions

Myocardial alterations concurrently occurred with mild CKD-MBD and comprised interstitial and perivascular fibrosis, as well as intramyocardial artery media thickening, preceding cardiomyocyte hypertrophy. The histological features of MR associated with myocardial P accumulation in settings of low bone turnover, prior to the increase in systemic Pi-regulating factors and with alterations in calcineurin, included ERK1/2, Notch, BMP, and Hedgehog gene expression profiles.

Supplementary Materials: The following supporting information can be downloaded at: <https://www.mdpi.com/article/10.3390/kidneydial3040028/s1>, Figure S1: Chronic kidney injury in applied models: (A)—the concentration of serum creatinine, (B)—albumin to creatinine ratio, (C)—quantitative morphometry for the area of interstitial fibrosis; (D)—representative microphotographs for Masson’s trichrome (upper line) and PAS staining (middle and lower lines) of left kidneys in normotensive rats (WKY2), hypertension (SO2, SO6), hypertension with 3/4 nephrectomy (Nx2, and Nx6); Figure S2: Static bone histomorphometry parameters: (A)—trabecular bone area (B.Ar/T.Ar), (B)—osteocyte number (N.Ot/T.Ar), (C)—osteoblast number (N.Ob/B.Pm), (D)—osteoclast number (N.Oc/B.Pm), (E)—eroded perimeter (E.Pm/B.Pm), (F)—the ratio of bone marrow cells area to adipose area; (G)—representative microphotographs for the bone morphometry parameters (H&E; arrowheads point osteoblasts, osteoclasts, eroded perimeter and vessels at the corresponded pictures; Figure S3: mRNA relative expression in bone: (A)—*Sp7*, transcription factor osterix; (B)—*Ctnnb1*, catenin beta 1; (C)—*Bmp4*, bone morphogenetic protein 4; (D)—*Vdr*, vitamin D receptor; (E)—*Tnfrsf11*, TNF superfamily member 11 (RANKL); (F)—*Tnfrsf11b*, TNF receptor superfamily member 11B (OPG); (G)—*Tnfrsf11* to *Tnfrsf11b* ratio; Figure S4: Representative micro photographs of von Kossa staining for groups studied. Table S1: Studies of bone and/or cardiovascular remodeling in rodent models of CKD-MBD; Table S2: Primer and probe sequences for RT-PCR; Table S3: Description of experimental groups.

Author Contributions: Conceptualization, E.B. and V.D.; methodology, E.B., A.S., V.S., I.Z., O.B., G.I. and M.P.; validation, O.G.; formal analysis, E.B.; investigation, E.B.; resources, E.B., A.S. and V.D.; data curation, I.Z.; writing—original draft preparation, E.B.; writing—review and editing, V.D.; visualization, E.B. and A.S.; supervision, E.B.; project administration, E.B.; funding acquisition, V.D. and E.B. All authors have read and agreed to the published version of the manuscript.

Funding: This research was funded by the Russian Foundation for Basic Research, grant number 18-315-00342 and 18-015-00425.

Institutional Review Board Statement: The animal study protocol was approved by the local Ethics Committee of Pavlov University (animal ethics approval code No. 02-2013, 23 April 2018).

Informed Consent Statement: Not applicable.

Data Availability Statement: All data presented in this study are available from the corresponding author on reasonable request.

Conflicts of Interest: The authors declare no conflict of interest. The funders had no role in the design of the study, in the collection, analysis, or interpretation of data, in the writing of the manuscript, or in the decision to publish the results.

References

1. Go, A.S.; Chertow, G.M.; Fan, D.; McCulloch, C.E.; Hsu, C.Y. Chronic kidney disease and the risks of death, cardiovascular events, and hospitalization. *N. Engl. J. Med.* **2004**, *351*, 1296–1305. [[CrossRef](#)] [[PubMed](#)]
2. Jankowski, J.; Floege, J.; Fliser, D.; Böhm, M.; Marx, N. Cardiovascular Disease in Chronic Kidney Disease: Pathophysiological Insights and Therapeutic Options. *Circulation* **2021**, *143*, 1157–1172. [[CrossRef](#)] [[PubMed](#)]
3. Blecker, S.; Matsushita, K.; Köttgen, A.; Loehr, L.R.; Bertoni, A.G.; Boulware, L.E.; Coresh, J. High-normal albuminuria and risk of heart failure in the community. *Am. J. Kidney Dis.* **2011**, *58*, 47–55. [[CrossRef](#)] [[PubMed](#)]
4. Parfrey, P.S.; Harnett, J.D.; Griffiths, S.M.; Taylor, R.; Hand, J.; King, A.; Barre, P.E. The clinical course of left ventricular hypertrophy in dialysis patients. *Nephron* **1990**, *55*, 114–120. [[CrossRef](#)]
5. Levin, A.; Singer, J.; Thompson, C.R.; Ross, H.; Lewis, M. Prevalent left ventricular hypertrophy in the predialysis population: Identifying opportunities for intervention. *Am. J. Kidney Dis.* **1996**, *27*, 347–354. [[CrossRef](#)]
6. Xie, J.; Yoon, J.; An, S.W.; Kuro-o, M.; Huang, C.L. Soluble Klotho Protects against Uremic Cardiomyopathy Independently of Fibroblast Growth Factor 23 and Phosphate. *J. Am. Soc. Nephrol.* **2015**, *26*, 1150–1160. [[CrossRef](#)]
7. Buckalew, V.M., Jr.; Berg, R.L.; Wang, S.R.; Porush, J.G.; Rauch, S.; Schulman, G. Prevalence of hypertension in 1795 subjects with chronic renal disease: The modification of diet in renal disease study baseline cohort. Modification of Diet in Renal Disease Study Group. *Am. J. Kidney Dis.* **1996**, *28*, 811–821. [[CrossRef](#)]
8. Nadruz, W. Myocardial remodeling in hypertension. *J. Hum. Hypertens.* **2015**, *29*, 1–6. [[CrossRef](#)]
9. Silberberg, J.S.; Barre, P.E.; Prichard, S.S.; Sniderman, A.D. Impact of left ventricular hypertrophy on survival in end-stage renal disease. *Kidney Int.* **1989**, *36*, 286–290. [[CrossRef](#)]
10. London, G.M. Left ventricular alterations and end-stage renal disease. *Nephrol. Dial. Transplant.* **2002**, *17* (Suppl. S1), 29–36. [[CrossRef](#)]
11. Williams, M.J.; White, S.C.; Joseph, Z.; Hruska, K.A. Updates in the chronic kidney disease-mineral bone disorder show the role of osteocytic proteins, a potential mechanism of the bone-Vascular paradox, a therapeutic target, and a biomarker. *Front. Physiol.* **2023**, *14*, 1120308. [[CrossRef](#)] [[PubMed](#)]
12. Drüeke, T.B.; Massy, Z.A. Changing bone patterns with progression of chronic kidney disease. *Kidney Int.* **2016**, *89*, 289–302. [[CrossRef](#)] [[PubMed](#)]
13. Ferreira, J.C.; Ferrari, G.O.; Neves, K.R.; Cavallari, R.T.; Dominguez, W.V.; dos Reis, L.M.; Gracioli, F.G.; Oliveira, E.C.; Liu, S.; Sabbagh, Y.; et al. Effects of dietary phosphate on adynamic bone disease in rats with chronic kidney disease—Role of sclerostin? *PLoS ONE* **2013**, *8*, e79721. [[CrossRef](#)] [[PubMed](#)]
14. Iwasaki-Ishizuka, Y.; Yamato, H.; Nii-Kono, T.; Kurokawa, K.; Fukagawa, M. Downregulation of parathyroid hormone receptor gene expression and osteoblastic dysfunction associated with skeletal resistance to parathyroid hormone in a rat model of renal failure with low turnover bone. *Nephrol. Dial. Transplant.* **2005**, *20*, 1904–1911. [[CrossRef](#)] [[PubMed](#)]
15. Fang, Y.; Ginsberg, C.; Seifert, M.; Agapova, O.; Sugatani, T.; Register, T.C.; Freedman, B.I.; Monier-Faugere, M.-C.; Malluche, H.; Hruska, K.A. CKD-induced wingless/integration1 inhibitors and phosphorus cause the CKD-mineral and bone disorder. *J. Am. Soc. Nephrol.* **2014**, *25*, 1760–1773. [[CrossRef](#)] [[PubMed](#)]
16. Magnusson, P.; Sharp, C.A.; Magnusson, M.; Risteli, J.; Davie, M.W.; Larsson, L. Effect of chronic renal failure on bone turnover and bone alkaline phosphatase isoforms. *Kidney Int.* **2001**, *60*, 257–265. [[CrossRef](#)] [[PubMed](#)]
17. Nickolas, T.L.; Stein, E.M.; Dworakowski, E.; Nishiyama, K.K.; Komandah-Kosseh, M.; Zhang, C.A.; McMahon, D.J.; Liu, X.S.; Boutroy, S.; Cremers, S.; et al. Rapid cortical bone loss in patients with chronic kidney disease. *J. Bone Miner. Res.* **2013**, *28*, 1811–1820. [[CrossRef](#)]
18. Tasnim, N.; Dutta, P.; Nayeem, J.; Masud, P.; Ferdousi, A.; Ghosh, A.S.; Hossain, M.; Rajia, S.; Kubra, K.T.; Sakibuzzaman, M.; et al. Osteoporosis, an Inevitable Circumstance of Chronic Kidney Disease: A Systematic Review. *Cureus* **2021**, *13*, e18488. [[CrossRef](#)]
19. Malluche, H.H.; Ritz, E.; Lange, H.P.; Kutschera, J.; Hodgson, M.; Seiffert, U.; Schoeppe, W. Bone histology in incipient and advanced renal failure. *Kidney Int.* **1976**, *9*, 355–362. [[CrossRef](#)]

20. Raggi, P.; Bellasi, A.; Bushinsky, D.; Bover, J.; Rodriguez, M.; Ketteler, M.; Sinha, S.; Salcedo, C.; Gillotti, K.; Padgett, C.; et al. Slowing Progression of Cardiovascular Calcification with SNF472 in Patients on Hemodialysis: Results of a Randomized Phase 2b Study. *Circulation* **2020**, *141*, 728–739. [[CrossRef](#)]
21. Ogata, H.; Fukagawa, M.; Hirakata, H.; Kagimura, T.; Fukushima, M.; Akizawa, T.; LANDMARK Investigators and Committees. Effect of Treating Hyperphosphatemia with Lanthanum Carbonate vs Calcium Carbonate on Cardiovascular Events in Patients with Chronic Kidney Disease Undergoing Hemodialysis: The LANDMARK Randomized Clinical Trial. *JAMA* **2021**, *325*, 1946–1954. [[CrossRef](#)] [[PubMed](#)]
22. Sutherland, J.P.; Zhou, A.; Hyppönen, E. Vitamin D Deficiency Increases Mortality Risk in the UK Biobank: A Nonlinear Mendelian Randomization Study. *Ann. Intern. Med.* **2022**, *175*, 1552–1559. [[CrossRef](#)] [[PubMed](#)]
23. Malluche, H.H.; Mawad, H.W.; Monier-Faugere, M.C. Renal osteodystrophy in the first decade of the new millennium: Analysis of 630 bone biopsies in black and white patients. *J. Bone Miner. Res.* **2011**, *26*, 1368–1376. [[CrossRef](#)] [[PubMed](#)]
24. Sprague, S.M.; Bellorin-Font, E.; Jorgetti, V.; Carvalho, A.B.; Malluche, H.H.; Ferreira, A.; D’Haese, P.C.; Drüeke, T.B.; Du, H.; Manley, T. Diagnostic accuracy of bone turnover markers and bone histology in patients with CKD treated by dialysis. *Am. J. Kidney Dis.* **2016**, *67*, 559–566. [[CrossRef](#)]
25. El-Husseini, A.; Abdalbary, M.; Lima, F.; Issa, M.; Ahmed, M.-T.; Winkler, M.; Srour, H.; Davenport, D.; Wang, G.; Faugere, M.-C. Low turnover renal osteodystrophy with abnormal bone quality and vascular calcification in patients with mild-to-moderate CKD. *Kidney Int. Rep.* **2022**, *7*, 1016–1026. [[CrossRef](#)] [[PubMed](#)]
26. Smogorzewski, M.; Zayed, M.; Zhang, Y.B.; Roe, J.; Massry, S.G. Parathyroid hormone increases cytosolic calcium concentration in adult rat cardiac myocytes. *Am. J. Physiol.* **1993**, *264 Pt 2*, H1998–H2006. [[CrossRef](#)]
27. Maulik, S.K.; Mishra, S. Hypertrophy to failure: What goes wrong with the fibers of the heart? *Indian Heart J.* **2015**, *67*, 66–69. [[CrossRef](#)]
28. Intengan, H.D.; Schiffrin, E.L. Vascular remodeling in hypertension: Roles of apoptosis, inflammation, and fibrosis. *Hypertension* **2001**, *38 Pt 2*, 581–587. [[CrossRef](#)]
29. Korsgaard, N.; Mulvany, M.J. Cellular hypertrophy in mesenteric resistance vessels from renal hypertensive rats. *Hypertension* **1988**, *12*, 162–167. [[CrossRef](#)]
30. Molkentin, J.D.; Lu, J.R.; Antos, C.L.; Markham, B.; Richardson, J.; Robbins, J.; Grant, S.R.; Olson, E.N. A calcineurin-dependent transcriptional pathway for cardiac hypertrophy. *Cell* **1998**, *93*, 215–228. [[CrossRef](#)]
31. Bacmeister, L.; Schwarzl, M.; Warnke, S.; Stoffers, B.; Blankenberg, S.; Westermann, D.; Lindner, D. Inflammation and fibrosis in murine models of heart failure. *Basic Res. Cardiol.* **2019**, *114*, 19. [[CrossRef](#)]
32. Shimizu, I.; Minamino, T. Physiological and pathological cardiac hypertrophy. *J. Mol. Cell Cardiol.* **2016**, *97*, 245–262. [[CrossRef](#)]
33. Liu, Y.-L.; Huang, C.-C.; Chang, C.-C.; Chou, C.-Y.; Lin, S.-Y.; Wang, I.-K.; Hsieh, D.J.-Y.; Jong, G.-P.; Huang, C.-Y.; Wang, C.-M. Hyperphosphate-Induced Myocardial Hypertrophy through the GATA-4/NFAT-3 Signaling Pathway Is Attenuated by ERK Inhibitor Treatment. *CardioRenal Med.* **2015**, *5*, 79–88. [[CrossRef](#)] [[PubMed](#)]
34. Bogdanova, E.; Beresneva, O.; Galkina, O.; Zubina, I.; Ivanova, G.; Parastaeva, M.; Semenova, N.; Dobronravov, V. Myocardial Hypertrophy and Fibrosis Are Associated with Cardiomyocyte Beta-Catenin and TRPC6/Calcineurin/NFAT Signaling in Spontaneously Hypertensive Rats with 5/6 Nephrectomy. *Int. J. Mol. Sci.* **2021**, *22*, 4645. [[CrossRef](#)] [[PubMed](#)]
35. Gross, M.L.; Ritz, E. Hypertrophy and fibrosis in the cardiomyopathy of uremia—beyond coronary heart disease. *Semin. Dial.* **2008**, *21*, 308–318. [[CrossRef](#)] [[PubMed](#)]
36. Creemers, E.E.; Pinto, Y.M. Molecular mechanisms that control interstitial fibrosis in the pressure-overloaded heart. *Cardiovasc. Res.* **2011**, *89*, 265–272. [[CrossRef](#)]
37. Weber, K.T.; Brilla, C.G. Pathological hypertrophy and cardiac interstitium. Fibrosis and renin-angiotensin-aldosterone system. *Circulation* **1991**, *83*, 1849–1865. [[CrossRef](#)]
38. *Code of Practice for the Housing and Care of Animals Bred, Supplied or Used for Scientific Purposes Presented to Parliament Pursuant to Section 21 (5) of the Animals (Scientific Procedures) ACT 1986*; Home Office: London, UK, 2014.
39. *Directive 2010/63/EU of the European Parliament and of the Council*; Official Journal of the European Union, Publications Office of the European Union: Luxembourg, 2020.
40. *Guide for the Care and Use of Laboratory Animals, 8th edition National Research Council (US) Committee for the Update of the Guide for the Care and Use of Laboratory Animals*; National Academies Press (US): Washington, DC, USA, 2011.
41. Lee, H.B.; Blaufox, M.D. Blood volume in the rat. *J. Nucl. Med.* **1985**, *26*, 72–76.
42. Fleischer, H.; Vorberg, E.; Thurow, K.; Warkentin, M.; Behrend, D. Determination of Calcium and Phosphorus in Bones Using Microwave Digestion and ICP-MS. In *Imeko Tc19 Symp*, 5th ed.; International Measurement Confederation (IMEKO): Lecce, Italy, 2014; ISBN 978-92-990073-6-5.
43. Erben, R.G.; Glösmann, M. Histomorphometry in Rodents. In *Bone Research Protocols. Methods in Molecular Biology*; Idris, A., Ed.; Humana Press: New York, NY, USA, 2019; Volume 1914.
44. Dempster, D.W.; Compston, J.E.; Drezner, M.K.; Glorieux, F.H.; Kanis, J.A.; Malluche, H.; Meunier, P.J.; Ott, S.M.; Recker, R.R.; Parfitt, A.M. Standardized nomenclature, symbols, and units for bone histomorphometry: A 2012 update of the report of the ASBMR Histomorphometry Nomenclature Committee. *J. Bone Miner. Res.* **2013**, *28*, 2–17. [[CrossRef](#)]
45. Aoki, J.; Ikari, Y.; Nakajima, H.; Mori, M.; Sugimoto, T.; Hatori, M.; Tanimoto, S.; Amiya, E.; Hara, K. Clinical and pathologic characteristics of dilated cardiomyopathy in hemodialysis patients. *Kidney Int.* **2005**, *67*, 333–340. [[CrossRef](#)]

46. Law, J.P.; Pickup, L.; Pavlovic, D.; Townend, J.N.; Ferro, C.J. Hypertension and cardiomyopathy associated with chronic kidney disease: Epidemiology, pathogenesis and treatment considerations. *J. Hum. Hypertens.* **2023**, *37*, 1–19. [[CrossRef](#)] [[PubMed](#)]
47. Mark, P.B.; Johnston, N.; Groenning, B.A.; Foster, J.E.; Blyth, K.G.; Martin, T.N.; Steedman, T.; Dargie, H.J.; Jardine, A.G. Redefinition of uremic cardiomyopathy by contrast-enhanced cardiac magnetic resonance imaging. *Kidney Int.* **2006**, *69*, 1839–1845. [[CrossRef](#)] [[PubMed](#)]
48. Wang, M.; Zhang, J.; Kalantar-Zadeh, K.; Chen, J. Focusing on Phosphorus Loads: From Healthy People to Chronic Kidney Disease. *Nutrients* **2023**, *15*, 1236. [[CrossRef](#)] [[PubMed](#)]
49. Bevington, A.; Mundy, K.I.; Yates, A.J.; Kanis, J.A.; Russell, R.G.; Taylor, D.J.; Rajagopalan, B.; Radda, G.K. A study of intracellular orthophosphate concentration in human muscle and erythrocytes by ³¹P nuclear magnetic resonance spectroscopy and selective chemical assay. *Clin. Sci.* **1986**, *71*, 729–735. [[CrossRef](#)]
50. Chazot, G.; Lemoine, S.; Kocevar, G.; Kalbacher, E.; Sappey-Marinié, D.; Rouvière, O.; Juillard, L. Intracellular Phosphate and ATP Depletion Measured by Magnetic Resonance Spectroscopy in Patients Receiving Maintenance Hemodialysis. *J. Am. Soc. Nephrol.* **2021**, *32*, 229–237. [[CrossRef](#)] [[PubMed](#)]
51. Polovlkova, O.G.; Makeeva, O.A.; Lezhnev, A.A.; Goncharova, I.A.; Kulish, E.V.; Shipulin, V.M.; Puzyrev, V.P. Expression profile of calcineurin pathway genes in myocardium tissues in relation to ischemic heart remodeling in humans. *Mol. Biol.* **2013**, *47*, 433–440. (In Russian)
52. Heineke, J.; Wollert, K.C.; Osinska, H.; Sargent, M.A.; York, A.J.; Robbins, J.; Molkentin, J.D. Calcineurin protects the heart in a murine model of dilated cardiomyopathy. *J. Mol. Cell Cardiol.* **2010**, *48*, 1080–1087. [[CrossRef](#)]
53. Ha, S.W.; Park, J.; Habib, M.M.; Beck, G.R., Jr. Nano-Hydroxyapatite Stimulation of Gene Expression Requires Fgf Receptor, Phosphate Transporter, and Erk1/2 Signaling. *ACS Appl. Mater. Interfaces* **2017**, *9*, 39185–39196. [[CrossRef](#)]
54. Bon, N.; Couasnay, G.; Bourguin, A.; Sourice, S.; Beck-Cormier, S.; Guicheux, J.; Beck, L. Phosphate (Pi)-regulated heterodimerization of the high-affinity sodium-dependent Pi transporters PiT1/Slc20a1 and PiT2/Slc20a2 underlies extracellular Pi sensing independently of Pi uptake. *J. Biol. Chem.* **2018**, *293*, 2102–2114. [[CrossRef](#)]
55. Szeri, F.; Niaziyori, F.; Donnelly, S.; Fariha, N.; Tertyshnaia, M.; Patel, D.; Lundkvist, S.; Wetering, K. The Mineralization Regulator ANKH Mediates Cellular Efflux of ATP, Not Pyrophosphate. *J. Bone Miner. Res.* **2022**, *37*, 1024–1031. [[CrossRef](#)]
56. Huang, C.K.; Dai, D.; Xie, H.; Zhu, Z.; Hu, J.; Su, M.; Liu, M.; Lu, L.; Shen, W.; Ning, G.; et al. Lgr4 Governs a Pro-Inflammatory Program in Macrophages to Antagonize Post-Infarction Cardiac Repair. *Circ. Res.* **2020**, *127*, 953–973. [[CrossRef](#)] [[PubMed](#)]
57. Brayden, D.J.; Alonso, M.J. Oral delivery of peptides: Opportunities and issues for translation. *Adv. Drug Deliv. Rev.* **2016**, *106*, 193–195. [[CrossRef](#)]
58. Shao, J.S.; Cai, J.; Towler, D.A. Molecular mechanisms of vascular calcification: Lessons learned from the aorta. *Arterioscler. Thromb. Vasc. Biol.* **2006**, *26*, 1423–1430. [[CrossRef](#)] [[PubMed](#)]
59. Rathinavel, A.; Sankar, J.; Mohammed Sadullah, S.S.; Niranjali Devaraj, S. Oligomeric proanthocyanidins protect myocardium by mitigating left ventricular remodeling in isoproterenol-induced postmyocardial infarction. *Fundam. Clin. Pharmacol.* **2018**, *32*, 51–59. [[CrossRef](#)] [[PubMed](#)]
60. Sun, B.; Huo, R.; Sheng, Y.; Li, Y.; Xie, X.; Chen, C.; Liu, H.B.; Li, N.; Li, C.B.; Guo, W.T.; et al. Bone morphogenetic protein-4 mediates cardiac hypertrophy, apoptosis, and fibrosis in experimentally pathological cardiac hypertrophy. *Hypertension* **2013**, *61*, 352–360. [[CrossRef](#)] [[PubMed](#)]
61. Dave, R.K.; Ellis, T.; Toumpas, M.C.; Robson, J.P.; Julian, E.; Adolphe, C.; Bartlett, P.F.; Cooper, H.M.; Reynolds, B.A.; Wainwright, B.J. Sonic hedgehog and notch signaling can cooperate to regulate neurogenic divisions of neocortical progenitors. *PLoS ONE* **2011**, *6*, e14680. [[CrossRef](#)]
62. Zhang, K.; Zhang, Y.Q.; Ai, W.B.; Hu, Q.T.; Zhang, Q.J.; Wan, L.Y.; Wang, X.L.; Liu, C.B.; Wu, J.F. Hes1, an important gene for activation of hepatic stellate cells, is regulated by Notch1 and TGF- β /BMP signaling. *World J. Gastroenterol.* **2015**, *21*, 878–887. [[CrossRef](#)]
63. Ingram, W.J.; McCue, K.I.; Tran, T.H.; Hallahan, A.R.; Wainwright, B.J. Sonic Hedgehog regulates Hes1 through a novel mechanism that is independent of canonical Notch pathway signalling. *Oncogene* **2008**, *27*, 1489–1500. [[CrossRef](#)]
64. Wang, G.; Zhang, Z.; Xu, Z.; Yin, H.; Bai, L.; Ma, Z.; Decoster, M.A.; Qian, G.; Wu, G. Activation of the sonic hedgehog signaling controls human pulmonary arterial smooth muscle cell proliferation in response to hypoxia. *Biochim. Biophys. Acta* **2010**, *1803*, 1359–1367. [[CrossRef](#)]
65. Katoh, M.; Katoh, M. NUMB is a break of WNT-Notch signaling cycle. *Int. J. Mol. Med.* **2006**, *18*, 517–521. [[CrossRef](#)]
66. Ortega-Campos, S.M.; García-Heredia, J.M. The Multitasker Protein: A Look at the Multiple Capabilities of NUMB. *Cells* **2023**, *12*, 333. [[CrossRef](#)] [[PubMed](#)]

Disclaimer/Publisher’s Note: The statements, opinions and data contained in all publications are solely those of the individual author(s) and contributor(s) and not of MDPI and/or the editor(s). MDPI and/or the editor(s) disclaim responsibility for any injury to people or property resulting from any ideas, methods, instructions or products referred to in the content.